On the model flexibility of the geographical distributed real-time co-simulation: The example of ENET-RT lab

Sustainable Energy, Grids and Networks 40 (2024) 101501

Contents lists available at ScienceDirect

Sustainable Energy, Grids and Networks

journal homepage: www.elsevier.com/locate/segan

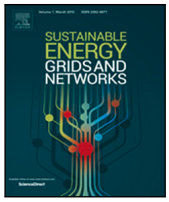

On the model flexibility of the geographical distributed real-time co-simulation: The example of ENET-RT lab

A. Mazza [a,*], G. Benedetto [a], E. Pons [a], E. Bompard [a], A. De Paola [b], D. Thomas [b,1], E. Kotsakis [b], G. Fulli [b], S. Vogel [c], A. Acosta Gil [d], A. Monti [d], S. Bruno [e], C. Iurlaro [e], M. La Scala [e], A. Bonfiglio [f], P. Cepollini [f], F. D'Agostino [f], M. Invernizzi [f], M. Rossi [f], F. Silvestro [f], F. De Caro [g], G. Giannoccaro [h], D. Villacci [h]

[a] *Department of Energy, Politecnico di Torino, Torino, Italy*
[b] *Smart Grid Interoperability Laboratory, Joint Research Centre - European Commission, Via Enrico Fermi 2749, Ispra, 21027, Italy*
[c] *OPAL-RT Germany, Aachen, Germany*
[d] *Institute for Automation of Complex Power Systems RWTH Aachen University Aachen, Aachen, Germany*
[e] *Department of Electrical & Information Engineering Politecnico di Bari, Bari, Italy*
[f] *Electrical, Electronics & Telecom. Eng and Naval Architecture, Dep. Università di Genova, Genova, Italy*
[g] *Department of Engineering. Università del Sannio, Benevento, Italy*
[h] *Department of industrial Engineering. Università di Napoli Federico II, Napoli, Italy*

ARTICLE INFO

Keywords:
Real time co-simulation
Power hardware-in-the-loop
Software-in-the-loop
Control-in-the-loop
Frequency control

ABSTRACT

The decarbonization of the energy sector represents a challenge that requires new tools and approaches of analysis. This paper aims to demonstrate the fundamental role that geographical distributed real-time co-simulations (GD-RTDS) can play in this regard. To this end, three different case studies have been analyzed with GD-RTDS, covering a wide range of applications for the energy sector decarbonization: (a) implementation of Renewable Energy Communities for supporting the share increase of Renewable Energy Sources, (b) the integration and management of Onshore Power Supply, and (c) the integration of a forecasting tool for the management of the Electric Vehicle charging. The performed experiments included fully simulated components, together with (power) hardware-in-the-loop and software-in-the-loop elements. These components have been simulated in different laboratory facilities in Italy and Germany, all operating in a synchronized manner under the presented geographically-distributed setup. The results show that the proposed architecture is flexible enough to be used for modeling all the different case studies; moreover, they highlight the significant contribution that the GD-RTDS methodology can give in informing and driving energy transition policies and the fundamental role of power systems to spearhead the complete decarbonization of the energy sector.

Nomenclature

AC Alternate Current

AFE Active Front End

AFIR Alternative Fuels Infrastructure Regulation

AVR Automatic Voltage Regulator

BESS Battery Energy Storage System

BEV Battery Electric Vehicle

CI Cold Ironing

CIL Control-in-the-Loop

DC Direct Current

DER Distributed Energy Resources

SG Synchronous Generator

DRTS Digital Real-Time Simulator

DSO Distribution System Operator

* Corresponding author.
E-mail address: andrea.mazza@polito.it (A. Mazza).
[1] D. Thomas is currently with the European Climate, Infrastructure and Environment Executive Agency (CINEA).

https://doi.org/10.1016/j.segan.2024.101501
Received 6 May 2024; Received in revised form 24 July 2024; Accepted 7 August 2024
Available online 13 August 2024

EMS Energy Management System

EV Electric Vehicle

EVSE Electric Vehicle Supply Equipment

GA Genetic Algorithm

GARR Gestione Ampliamento Rete Ricerca

GD-CHIL Geographical Distributed Controller-Hardware-in-the-Loop

GD-HIL Geographical Distributed Hardware-in-the-Loop

GD-PHIL Geographical Distributed Power-Hardware-in-the-Loop

GD-RTS Geographical Distributed Real Time Simulation

G2V Grid-to-Vehicle

GFL Grid-Following

GFM Grid-Forming

HEMS Home Energy Management Systems

MV Medium Voltage

HIL Hardware-in-the-Loop

HVSC High Voltage Shore-Connection

ICT Information & Communication Technology

IEC International Electrotechnical Commission

ITM Ideal Transformer Model

JRC Joint Research Centre

LEM Local Energy Market

LV Low Voltage

NAT Network Address Translation

OPS Onshore Power Supply

PHIL Power Hardware-in-the-Loop

PV Photovoltaic

REC Renewable Energy Community

RES Renewable Energy Sources

RI Research Infrastructure

RoCoF Rate of Change of Frequency

RT Real-Time

RTS Real-time Simulation

SPS Ship Power System

SIL Software-in-the-Loop

SoC State of Charge

SVM Support Vector Machine

UDP User Datagram Protocol

V2G Vehicle-to-Grid

VPN Virtual Power Network

VSC Voltage Source Converter

VSI Voltage Source Inverter

1. Introduction

The energy transition calls for a shift from fossil primary sources to Renewable Energy Sources (RES). In fact, the public awareness about the effects of the climate change has increased over the last decades, leading policy makers to introduce new frameworks for boosting the share of RES in the whole energy system, expanding the electrification of demand [1], promoting new forms of consumers engagement such as RECs, and strengthening *sector coupling* [2]. This latest action is also meant to support the decarbonization of carbon-intensive sectors such as transportation [3] (including both land and non-land transport means).

1.1. Role of RECs and transport for the decarbonization

RECs are commonly envisioned as a key enabling step to achieve an inclusive and efficient decarbonization of the energy system. RECs have been formally introduced in the European legislative framework with the Directive 2001/2018 (RED II) [4], which emphasizes the provision of environmental, economic and social community benefits (rather than economic profits) as the primary mission of RECs. The implementation of the RED II directive and the roll-out of RECs is being carried out in the Member States with different approaches and timelines [5]. There is the expectation the deployment of RECs will accelerate in the upcoming years and that, by 2050, RECs could own up to 17% and 21% of total wind and solar capacity, respectively, at a global level [6]. From a local perspective, RECs can provide direct benefits to citizens by improving the energy efficiency, lowering electricity bills and creating local job opportunities. They could ensure, with suitable support, fairly distributed benefits [7]. From a whole-system perspective, RECs can represent an important source of flexibility and can directly contribute to the operation of the low-inertia decarbonized energy system of the future. The research focused on developing forecast frameworks [8–10] and control schemes [11–13] for RECs; however, there has not been any assessment about their overall impact at a system level.

For what concerns the transport sector, a thorough analysis must consider the specific features of each of its different sub-sectors, such as land transport (light-duty and heavy-duty), shipping [14], and aviation. In particular, regarding charging infrastructure for land transport, most of the existing charging stations currently enable only unidirectional energy flows, i.e., the so called Grid-to-Vehicle (G2V) paradigm, where vehicles operate as passive loads. However, the availability of storage resources (i.e., the batteries of the vehicles) and the grid connection can enable the so-called Vehicle-to-Grid (V2G) paradigm, with bidirectional energy flows and the capability of providing grid support. It is worth noting that, currently, according to the charging modes described by the International Electrotechnical Commission (IEC) standard 61851-1:2018 [15], only the Charging Mode 4 supports the V2G paradigm. The proper integration of the chargers within the electrical grid must consider power quality aspects. For what concerns Europe, EN 50160 Standard specifies the main characteristics that the grid voltage should meet at the user's supply terminal [16]. The grid integration of EVs could have a potential impact on the power quality of the electrical system, according to the number of EVs charged at the same time, their location, the charging rate, and the time of the charging [17]. In [18] both the harmonics and supra-harmonics[2] content of a charging station in Netherlands have been analyzed: the harmonic and supra-harmonic emissions caused by nine different models of Battery Electric Vehicles (BEVs) have been studied and eight out of nine have proven to be source of supra-harmonics. Interactions between supra-harmonic currents can occur when two devices are connected close to each other. The Joint Research Centre (JRC) has conducted studies on the grid

[2] Supra-harmonics are defined in [19] as waveform distortions in the frequency range from 2 to 150 kHz.

harmonic impact of multiple EV fast charging [20], revealing that the phase angles between the same harmonic order tended to be lower than 90°, leading to summation of harmonics. This implies that there should be a maximum acceptable number of vehicles/chargers connected at the same grid infrastructure.

Regarding shipping and aviation, decarbonization must address two aspects: (*i*) the decarbonization of the means of transport themselves and (*ii*) the decarbonization of the auxiliary infrastructures, i.e., ports and airports. Both actions are considered within the European "Fit-for-55" package of directives. In this regard, the "FuelEU maritime" initiative, and the Alternative Fuels Infrastructure Regulation (AFIR) are particularly important for the maritime sector, as they include the electrification of ports as one of the foundation stones of the decarbonization process [21]. The key facility for ports electrification is the Cold Ironing (CI), also known as Onshore Power Supply (OPS). It enables ships to switch off their own generators while at berth, and withdrawn power by the inland grid through the so called shore-connection infrastructure. The main advantages include the drastic reduction of local air-polluting emission. The estimation of a port's power demand is deeply related to the CI load profile, i.e., the estimation of the ship's power demand. The CI power varies from hundreds of kW to tens of MW, depending on the type of ship to be supplied and its main characteristics, such as size and operating profile [22]. As a matter of example, cruise ships typically use High Voltage Shore-Connection (HVSC), with a rated power of 15 to 20 MW for each ship. In this scenario, the coordination between national system, ports, and ship operators is crucial to ensure smooth connection procedures and maintaining adequate performance at the system level.

1.2. Role of the power system in the energy transition and necessity of new tools

What mentioned so far demonstrates the "new" role of the power system as main player for enabling the energy transition: in fact, it is the system that enables the (virtually complete) decarbonization of the entire energy system, by proper managing the injection of RES. However, safe and reliable operation of the power system must be guaranteed while integrating larger and larger shares of non-dispatchable RES generation. In fact, the integration of RES is challenging, because solar and wind power plants are non-dispatchable (i.e., their output power basically depends on the primary source and cannot be controlled), and present small or null inertia. The reduction of the system inertia requires the implementation of fast frequency control by Distributed Energy Resources (DER), which rely on the design and tuning of advanced frequency controllers [23], proper modeling [24], and the experimental evidence of practical implementations [25,26]. It is important noting that both the sector coupling and the wide range of actions generally denoted as "demand-response" (hence, also in aggregated form, such as RECs [27]) can certainly support the proper operation of RES-based power system. However, assessing RES and DER control capabilities in decarbonized power systems requires the use of holistic approaches, capable of testing and validating a whole cyber–physical system, which includes not only the power grid and its power components, but also sensors, meters, on-line computing resources, controllers, and communication systems. It is therefore crucial to address the complexity and the impact of all the different participating elements, so that their full potential can be exploited. Due to the diversity of the facilities and of the technologies potentially involved, the modeling activity requires different competencies and backgrounds which may not all be available within a single research group. For this reason, this paper, which is an extension of [28], pools expertise and infrastructures of different European laboratories and adopts the GD-RTS paradigm to study the interactions between the power system and the new facilities in the energy transition framework. In this context, the use of GD-RTS has also the advantage of introducing real hardware, software and control systems within the experiment, by exploiting the so-called Power Hardware- (PHIL), Hardware- (HIL), Software- (SIL), and Control-in-the-Loop (CIL) configurations. This paper demonstrates the flexibility of the GD-RTS to test new systems and approaches supporting the decarbonization of the energy system by investigating three case studies:

1. the combined use of RECs, inertial provision by wind generators and demand response to increase flexibility and hence to enhance the stability of a "transition power system", where traditional power plants still exist, but the system presents a reduced control capability due to the decommissioning of some of them. This example was included in [28] and uses both PHIL and SIL configurations;
2. the modeling of a set of electrified quays, connected to the transmission system. This model aims to investigate the dynamics associated to the connection of the ship after its docking and its subsequent disconnection due to slipping moorings. In this case, only SIL is included.
3. the modeling of an EV parking, equipped with PV panels, aiming to control the power exchange with the local distribution grid. This case includes also a forecasting algorithm of the PV generation, so that the power used for charging the EVs may be properly modulated. This case includes SIL and PHIL configurations;

The paper is structured as follows: Section 2 presents the technical details of the GD-RT co-simulation; Section 3 shows the elementary components implemented by the different participating laboratories; Section 4 focuses on the case studies and their results; Section 5 presents some hints regarding the lessons learnt in the implementation of the simulation infrastructure; finally, Section 6 reports the concluding remarks.

2. Technical implementation of the GD-RT co-simulation

2.1. Basics of RTS technology

Real-time Simulation (RTS) represents nowadays an important stage in model-based design processes, especially for testing different devices before field tests [29]. This is done through the well-known CIL and PHIL concepts. The key advantage of RTS relies on the fact that one simulation time step matches the same amount of actual time, e.g., one second in the RTS corresponds to one second in reality. This behavior allows to emulate conditions which are very close to those of the actual power grid with an improved flexibility and scalability with respect to physical laboratory setups. RTS has been demonstrated to be particularly useful in the context of energy transition and decarbonization of the power grid, as many manufacturers, as well as an important number of Research Infrastructures (RIs), are interested on testing new technologies and novel control strategies and Energy Management System (EMS) aimed, for example, to guarantee the stable operation of the power systems. Moreover, increasing the scale of RTS scenarios imposes additional budgetary and organizational issues, since the majority of the simulation platforms require additional licenses to increase the number of simulation cores. These challenges motivated the idea of GD-RTS, which aims to extend the capabilities of several RIs by coupling their RTS platforms and hardware devices over a communications network. This makes GD-RTS a special case of co-simulation. Through this concept, the resources, expertise and existing setups of partner RIs are combined in order to analyze larger and more complex scenarios. Another advantage of the GD-RTS setup is the modularity and distributed implementation of the simulation models. The simulation data of the system module simulated in each RI is not disclosed with the others, by facilitating collaborations, and reducing the risks related to sharing of intellectual property. GD-RTS has evolved from a theoretical and practical perspective [30], starting from feasibility studies involving only two RIs and relying on custom-defined

solutions for data exchange [31], to the extension of the concept to Geographical Distributed Hardware-in-the-Loop (GD-HIL) in multi-RI experiments over continental distances [32], and the implementation of high-performance, flexible and multiprotocol communication gateways [33]. Regarding the applications, GD-RTS experiments have been reported for frequency regulation in large transmission systems [34], [35], voltage regulation of distribution networks [36] and control of microgrids [37].

The adoption of HIL configuration for port decarbonization has proven to be a powerful tool for the design and validation of cold ironing converters, their automation systems, and port Battery Energy Storage System (BESS) controllers. The work [38] presents a high-power supply network capable of supplying various types of ships with specific voltage and frequency requirements, thanks to its automation system which is developed and validated through HIL approach. The article [39] proposes a novel multipurpose cold ironing topology, which improves the power quality. Its control and automation system manages both ship and port power quality aspects, using HIL as a validation and testing tool. Finally, [40] presents a BESS controller developed to balance the mismatch between port power demand and supply. The controller is tested using IEC 61850 GOOSE messages in an HIL environment, utilizing real measurement data from Vaasa port.

The challenges of integrating electric vehicle chargers into electrical networks can be effectively studied by using RTS. Some sources identify the necessity of impacts analysis of the charging of EVs for power grids: in [41], the uncoordinated power absorption has been studied, evaluating also the injection of disturbances during the charging operations, as also made in the work [42]. In the document [43], the overloading of the system transformers and the distribution lines has been studied, while in [44] severe voltage drops and even blackouts problems have been investigated. PHIL approach has been effectively utilized to test and validate the performance of physical EV chargers and their interactions with the grid. Ref. [45] details a PHIL testbed that uses both a battery emulator and a grid emulator to simulate real-world scenarios. Similarly, ref. [41] explores the impact of various EV charging technologies on distribution networks, emphasizing the power quality aspects and the behavior of protection devices. Another significant area of study is the impact of EV charging algorithms on grid stability and voltage profiles. Refs. [43,44] provide insights about smart charging algorithms that can be developed and tested using PHIL setups. For instance, the reference [44] focuses on creating a PHIL testbed to implement and evaluate smart EV charging algorithms, while [43] presents a PHIL testbed that includes an actual EV and a custom Electric Vehicle Supply Equipment (EVSE), designed for realistic testing of charging algorithms under various grid conditions. The research presented in [46] describes an average model of a bidirectional charger integrated into a PHIL setup. This setup is used to study V2G strategies and their impact on residential distribution networks. In the case of energy communities, there are some examples implementing RTS. The work [47] presents a CIL setup for evaluating algorithms for Local Energy Markets (LEMs) based on Blockchain technology. A decentralized Genetic Algorithm (GA) is implemented in several Raspberry Pis, which act as Internet-of-things devices, to optimize the energy flow within the community and automate the trading processes. In [48], a co-simulation of a large scale low-voltage grid is implemented to investigate the impacts of energy communities incorporating a high penetration of BEVs and Home Energy Management Systems (HEMS). The authors introduce a middleware based on MQTT, namely “Lablink”, for message exchange and synchronization. Finally, the articles [49,50] present a GD-RTS testbed aimed for testing the interaction between RECs and transmission grids. The setup interconnects two laboratories in Germany, being the HIL laboratory at Forschungszentrum Jülich and the Energy Lab 2.0 laboratory at the Karlsruhe Institute of Technology. Communications are enabled using the VILLASframework toolkit [51], which is a real-time capable and flexible gateway supporting multiple general-purpose and power-system-oriented communications protocols.

3. Information about the basic co-simulation hardware and software elements

The case studies presented in this work are based on a number of models, control strategies and real equipment belonging and running in the different laboratories within a unique GD-RTS framework. Table 1 aims to provide a synthesis of the components, showing also the laboratory offering each of them. In the following, the reader can find a brief description of each component.

3.1. Component #1: Power system model

The power system model used in some of the presented cases aims to represent a *transitional* system, where a part of the traditional generation has been dismissed. In fact, even though the system is based on the CIGRE 12-bus transmissions system [52] shown in Fig. 1, the traditional generators installed at nodes 10 and 12 have been modified, as shown in Table 2.

These modifications have an impact on the system inertia, reducing its capability to face and overcome sudden power unbalances. Hence, to preserve the secure operation of the system, new resources and support features must be included.

3.2. Component #2: Renewable energy communities (RECs)

RECs are commonly envisioned as a key enabler for an efficient energy transition that delivers economic and social benefits to local communities. At the same time, they have the potential to leverage their flexibility to support power system operation, for example contributing to frequency regulation. In order to quantitatively investigate this latter element, two different types of RECs have been implemented in the GD-RTS setup. The modeling of the RECs is based on the Banshee distribution network, an established benchmark that is widely adopted in the context of RTS to assess advanced functionalities of microgrids [53]. The first type of REC has been derived from feeder #1 of the Banshee network and is equipped with a 400 kVA synchronous machine (to represent either a hydro or diesel generator) which is operated with a voltage and frequency droop control, envisaging a 4% linear droop. The REC is also equipped with a large 200 HP induction motor with compressor loads, which represents a critical non-interruptible load. The second type of REC has instead been derived from feeder #2 of the Banshee network and exhibits some significantly different characteristics. In particular, it is equipped with a 3 MW PV array and a 2.5 MVA BESS, both operated by inverter modules capable of four-quadrant operations. The BESS is not only controlled for power factor correction, peak shaving and smoothing, but it has also the capability of power export. Both types of RECs are equipped with protection elements on synchronism check, phase under-over voltage and phase overcurrent. The communities are connected to the main grid through circuit breakers that allow load-shedding disconnection.

3.3. Component #3: Real-time forecasting tool

3.3.1. Integration between artificial intelligence and real-time simulations

The application of artificial intelligence in power systems has gained tremendous popularity in power systems research and industry due to the combination of the increase in computational and data storage capability and the development of new complex algorithms, such as deep learning techniques [54]. Machine learning can be applied to several power-system tasks, from forecasting variable power generation/load profiles across different spatio-temporal scales to predict system state variables/detecting potential not-secure states. In more recent times, the research has also focused on meta-models, which try to emulate the behavior of more computational-intensive models, making their integration in RT operation easier [55].

Table 1
Synthesis of the experiment components.

Comp. #	Comp. name	Laboratory
1	Power System model	G-RTS*Lab* - Politecnico di Torino
2	Renewable Energy Communities	JRC Ispra (Type 1) and RWTH Aachen (Type 2)
3	RT Forecasting Tool	University of Sannio
4	RT Charging Station Management	G-RTS*Lab* - Politecnico di Torino
5	Measures from a real PV field	University of Genoa
6	Port Electrification model	University of Genoa
7	Wind Farm with inertial controller	University of Genoa
8	Microgrid with Flexible DERs (in PHIL)	LabZERO - Politecnico di Bari
9	Traditional Medium Voltage (MV) Grid	University of Naples "Federico II"

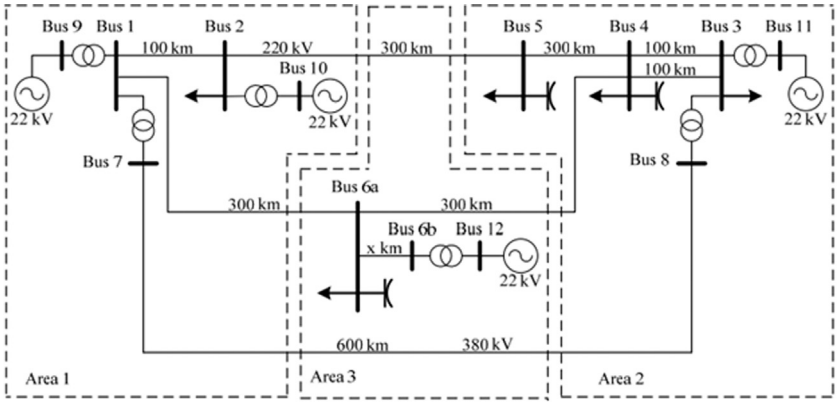

Fig. 1. 12-bus CIGRE transmission system [52].

Table 2
Modifications applied to the installed traditional generation.

Node	S_{orig} (MVA)	S_{mod} (MVA)
10	700	350
12	500	250

Generally, the development of machine-learning-based methodologies is confined to the offline testing stage, where all test data are already available and prompt to use, leaving the prototyping tasks to the industry. However, the integration of machine learning algorithms in a RT environment permits a more complete development, since the developers must face challenges linked to the stream data management (since not all the data are available in the same time steps), or because raw data must be processed since the algorithm adopts as input feature engineered variables.

Particularly, in this manuscript, a very short-term and multi-step PV power forecasting has been used, in which the prediction will be integrated into decision-making problems in the presence of uncertainty in real-time.

3.3.2. Base-workflow

The integration of artificial intelligence in RT simulation requires the usage of a certain set of blocks, which act iteratively over time (assigned a sampling time) or after a trigger event (user or system state condition-ruled). The type of addressed problem (regression or classification) may affect the used blocks. Generally, it is possible to recognize the following main blocks in a RT forecasting tool:

- *Time-Clock*: this block rules the input sample acquisition and output delivery with the assigned forecasting time resolution. It must not be confused with the solver's fixed step size;
- *Input Data Scaler*: to make the training process more effective and with a smoother gradient during the training process, a good idea is to reduce the range of input variables within a small range as $[0, 1]$. As a consequence, also the new input data must be scaled according to the scaling factors and the rules used in the training step;
- *Data Feature Generator and Embedder*: raw scaled input data can be processed to create engineered features processed by the trained predictor algorithm. This block depends on what type of learner has been deployed (machine learning or deep learning regressor). Engineered features may require the computation of moving mean, or moving percentile according to a fixed loop-back time window. In this case, a memory buffer is necessary to store the last observed samples to compute them. Furthermore, this block should consider rules to manage potential corrupted or missing data using a predefined strategy.
- *Forecasting Model*: this block performs the prediction given the set of inputs and according to the forecasting delivery sampling time.
- *Output Data Unscaler*: if the output data have been scaled in the training process, this block applies the inverse of the scaling function to make the data dimensional.
- *Output Filter*: due to the data-driven nature of the machine-learning model, they may be able to perfectly follow the physics of the observed process, or may be affected by excessive noise in the presence of multi-step and direct strategy forecasting. In this case, a set of filters are applied to solve these issues.
- *Performance Monitoring Tool*: it is a block that stores the outputs and compares them with the observed values in the future when they are observable. This block is crucial in ensemble or adaptive strategy since enables to update the weight for each of the models involved and the RT learning strategy to try to correct the forecasting model performance.

3.3.3. Mathematical formulation of the RT forecasting tool

Mathematically, the prediction method attempts to infer the values of the next H samples from the past samples at the t-th time step. Particularly, the adopted prediction strategy affects the type of used input samples [56]. In this specific case, a direct stage has been applied: for each time t, h models have been trained using the same knowledge stored in the set $\mathcal{X}_t$:

$$\hat{y}_{t+h} = f_h(\mathcal{X}_t) \tag{1}$$

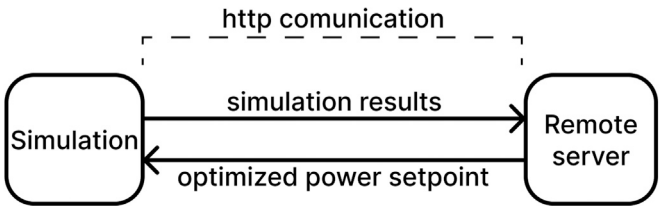

Fig. 2. Charging stations management integration structure.

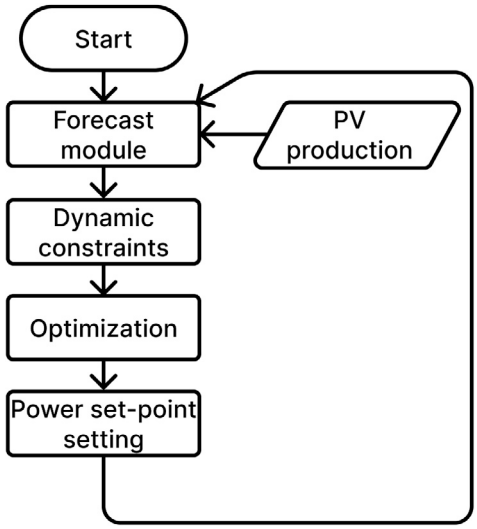

Fig. 3. Optimization logic.

where f_h is the h-th prediction model and $\mathcal{X}_t$ stores F variables such that:

$$\mathcal{X}_t = \{x_{1,t-d}, \dots, x_{1,t-d-L}, \dots, x_{F,t-d}, \dots, x_{F,t-d-L}\}, \tag{2}$$

where L and d are the number of loop-back variables and d is the delay of each variable.

3.4. Component #4: Charging stations management

In order to properly manage the charging station scenarios, the RT signal from a real PV and the signal from the forecasting tool need to be managed. The considered structure sees a node connected to the main grid, already supplying modulable load, at which six new models of electric vehicle chargers are added. Theoretically, the connection to the main grid should be upgraded in order to withstand the increased load. However, in our case, the system is managed in order to not exceed the original capacity through a smart charging approach coordinated with the local PV production.

The energy management system is based on a minimum cost optimization problem. This cost encompasses various components, including the cost of charging EVs, the cost associated with uncharged energy due to charging discontinuity, the load shedding cost, and the cost of purchasing energy from the grid. The optimization runs every time step, which is equal to one minute, so the trajectory of the optimized power can be adjusted in case of errors in the initial forecast, as schematically shown in Fig. 3. The cited algorithm works over a time horizon of five minutes, providing an operational schedule over such interval, then the power values scheduled for the first time step are applied. Rather than directly hard-coding the management system inside the model, the cited script is running on a separate server reachable from the simulator through a simple *http API* request in order to ensure a high modular structure, represented in Fig. 2. The objective function in Eq. (3) minimizes the cost of operating the service, taking into account the number of wall boxes or charging points n_{WB} and the number of time steps considered in the model n_{Time}. To compute the power balance, the power $p_{car_j}^{(G2V)}(t)$ transferred from the grid to the vehicle j at time t, the load $p^{(L)}(t)$ at time t, and the power input from the grid $p^{(GridIn)}(i)$ at time t are considered.

$$\min\left(-\sum_{j=0}^{n_{WB}}\sum_{t=0}^{n_{Time}} p_{car_j}^{(G2V)}(t)\cdot c_{ch} + \sum_{t}^{n_{Time}}(P_{max}^{(L)} - p^{(L)}(t))\cdot c_{curt} + \right. \\ \left. + \sum_{i=0}^{N} p^{(GridIn)}(i)\cdot c_{grid}\right) \tag{3}$$

where c_{ch}, c_{curt}, and c_{grid} represent the unit energy costs for vehicle charging (considered negative), load shedding, and energy purchased from the grid, respectively. The model is subject to various constraints: these include the energy balance (4) at every time step, ensuring that the charging power does not exceed the available PV power in (5).

$$p^{(L)}(t) - p^{(GridIn)}(t) - p^{(PV)}(t) + \sum_{j=0}^{n_{WB}} p_{car_j}^{(G2V)}(t) = 0 \quad \forall t \in [0, n_{Time}] \tag{4}$$

$$\sum_{j=0}^{n_{WB}} p_{car_j}^{(G2V)}(t) \le p^{(PV)}(t) \quad \forall t \in [0, n_{Time}] \tag{5}$$

The available power is then shared among the vehicles based on the maximum charging power of each vehicle through the k_j coefficient, computed as in (6), (7) and (8).

$$P_{tot} = \sum_{j}^{n_{WB}} P_{max}(j) \tag{6}$$

$$k_j = \frac{P_{max}}{P_{tot}} \tag{7}$$

$$p_{car_j}^{(G2V)}(t) \le k_j \cdot p^{(PV)}(t) \quad \forall j \in [0, n_{WB}], \forall t \in [0, n_{Time}] \tag{8}$$

with k_j being the proportion of the maximum power absorbable by vehicle j relative to the total power.

Additional constraints are applied to maintain the State of Charge (SoC) within specific limits ($SoC_{min,j}$ and $SoC_{max,j}$) for each vehicle and adhere in this way to the maximum charging power available, stated as $P_{ch,j}^{(Max)}(t)$. The SoC for each vehicle is updated at each timestep, ensuring that the charging process aligns with the EVs' operational and battery constraints as computed in (11) and (12):

$$SoC_{min,j}(t) \le SoC_{car_j}(t) \le SoC_{max,j}(t)\cdot \\ \forall j \in [0, n_{WB}], \forall t \in [0, n_{Time}] \tag{9}$$

$$p_{car_j}^{(G2V)}(t) \le P_{ch,j}^{(Max)}(t) \quad \forall j \in [0, n_{WB}], \forall t \in [0, n_{Time}] \tag{10}$$

- For $t > 0$:

$$SoC_{car_j}(t) = SoC_{car_j}(t-1) + (\tau \cdot (p_{car_j}^{(G2V)}(t)\cdot \eta^{(G2V)})) \\ \forall t \in [0, n_{Time}], \forall j \in [0, n_{WB}] \tag{11}$$

- For $t = 0$:

$$SoC_{car_j}(0) = SoC_{0,j} + (\tau \cdot (p_{car_j}^{(G2V)}(0)\cdot \eta^{(G2V)})) \\ \forall j \in [0, n_{WB}] \tag{12}$$

The proposed methodology highlights the importance of integrating detailed operational constraints and optimizing the charging process, paving the way for more efficient and cost-effective EV charging strategies.

3.5. Component #5: Measurements from a real PV field

The Savona Campus hosts a microgrid with a number of generators (PVs and gas-fired), controllable loads (a geothermal heat pump and an air handling unit), and a BESS. All the devices are connected to a SCADA system, which enables to supervise the entire infrastructure and store historical data. Each device can also be individually controlled and interfaced: for example, measurements can be collected from the 80 kW PV via a Modbus TCP interface. For the purposes of this paper, a Python script was used to collect the measured power from the PV field via Modbus; the data was then relayed to the GD-RTS infrastructure via a local Villas node. The RT measurements, properly scaled, were used to emulate a PV power injection in the transmission or distribution network.

3.6. Component #6: Port electrification model

The HVSC facility enables the CI of ships with a power demand of up to 15–20 MW. This facility typically comprises a conversion system, addressing the difference in frequencies between the SPS at 60 Hz and prevalent bulk grid frequency at 50 Hz. The conversion system is composed of two-stage static converters. The first stage is used to supply the common Direct Current (DC) bus; it can be a diode rectifier or an Active Front End (AFE) Voltage Source Converter (VSC). The second stage is a Voltage Source Inverter (VSI) used to generate the 60 Hz HVSC voltage. Fig. 4 shows the one line diagram and the control system of the HVSC. The first stage VSC is typically controlled employing a Grid-Following (GFL) control scheme. The direct-axis current reference is derived from the DC bus voltage controller, and the quadrature axis current reference is set to zero, or can be used for higher-level control strategies. The ship side VSC is controlled by means of a Grid-Forming (GFM) control scheme, as it needs to supply an isolated network. The second stage VSC is connected to the SPS through an insulation transformer selected and installed in accordance with the standard requirements [57]. The estimation of the total power demand foreseen for the Italian ports, assuming all berthed ships connect to the main grid, falls within the range of hundreds of megawatts. One of the most interesting study case is represented by the port of Genoa (Italy), among one of the major EU ports, with a potential yearly power demand ranging from 30 to 150 MW. Given the substantial magnitude of active power demand, coordinating shore connection among network system operators becomes imperative. This coordination necessitates collaboration between the port's Distribution System Operator (DSO) and the port microgrid operator during ship load transfers, representing a crucial measure to mitigate potential hazardous scenarios. When the ship is berthed, a single Synchronous Generator (SG) is turned on and connected to the ship grid through the SG switch. To ensure seamless connection to the port, the ship's connection needs to occur online. The typical connection procedure requires the SG to synchronize with the shore, HVSC switch closing and subsequently transferring the ship load to the HVSC [58]. Fig. 5 shows the SG control system. It consists of a speed governor for Diesel prime movers and an excitation system with an Automatic Voltage Regulator (AVR). The SG synchronization requires voltage magnitude, phase, and frequency measurements at both the HVSC and SG terminals of the shore-connection breaker. The measurements are used to achieve phase and voltage magnitude synchronism, so that when both HVSC and SG voltage are within a certain tolerance, the HVSC switch closes connecting the SPS to the inland grid. The Load Transfer regulator controls both the SG's active and reactive power, through additional signals provided to the governor and the AVR. Once the power is transferred to the shore-connection, the SG is switched off. The disconnection procedure follows the same steps in reverse order. The automation system synchronizes the SG to the HVSC voltage, the SG switch closes, and the ship's load power transfers from the HVSC to the SG. Once both the active and reactive power flowing into the HVSC switch reach a value close to zero, the HVSC switch opens disconnecting the ship from the HVSC.

3.7. Component #7: Wind farm equipped with an inertial controller

A wind farm with nominal power $P = 260$ MW is emulated with a Speedgoat that includes, in a HIL fashion, a prototype of an innovative inertial controller [59]. Its inertial controller enables to temporarily generate extra power by slowing down the rotating shafts of the generator, thus reducing the Rate of Change of Frequency (RoCoF) of critical frequency events whenever it reaches the threshold of 0.5 Hz/s.

3.8. Component #8: Microgrid with flexible distributed resources

This component allows to couple the RT co-simulation with the actual response of a physical microgrid, which is fully equipped with generation, load and storage flexible resources. The microgrid is coupled with the co-simulation thanks to a PHIL set-up [60]. A power amplifier reproduces, at the electrical busbars of the microgrid, the real-time voltage conditions experienced in the simulated system. The PHIL set-up also includes the emulation of controllers that can be programmed to enable the physical flexible resources to provide energy services, such as demand response [61], fast frequency response, synthetic inertia [25], etc.

In Case study #1, this PHIL co-simulation node is used to implement an automatic load shedding scheme, which disconnects a physical load once the frequency reaches a value lower than 49.5 Hz. This interruptible load is reconnected when the frequency rises back above 49.9 Hz.

3.9. Component #9: Traditional MV distribution grid

The MV distribution grid model has been elaborated to emulate a real electrical network based in Turin (Italy), used in other works as [62]. The size and the high number of real time measurement points in the complete model requires significant computational resources and a minimum time step of $100\mu s$. So in order to keep it running with the lowest time step possible, in the current work only a feeder of this the network was used, resulting in a 8-bus feeder. The network is modeled on real data provided by Turin DSO. In Fig. 6, a single-line representation of the electrical grid is given, with each node representing a MV to Low Voltage (LV) substation.

4. Case studies

This section aims to present the results of the three case studies under analysis. For the sake of clarity, Table 3 shows the components included in each case study.

4.1. Case study #1: Frequency regulation in low-inertia systems with support from RECs

The conceptual scheme of the experimental setup is shown in Fig. 7. The case study consists in a unique co-simulation composed of different subsystems, all connected to the transmission system by power transformers. This first case study aims to demonstrate the capability of the developed GD-RTS setup of simulating critical system conditions, providing an accurate characterization of the most relevant dynamics and phenomena. To this purpose, the simulation has considered a representative paradigm of a future decarbonized power system. The simulated grid exhibits low inertia, as a result of the dismissal of a non-negligible share of its synchronous generation park, and relies on renewable generators (i.e., inertial support from wind power plant as in [35]), together with regulation resources at distribution level (load disconnection and REC support), to adequately support the stability of the grid in case of severe frequency events. The RECs, characterized in Section 3.2, have been included in the model with a twofold aim: (*i*) verify their potential support to the bulk power system and (*ii*) demonstrate their capacity to overcome major contingencies in the

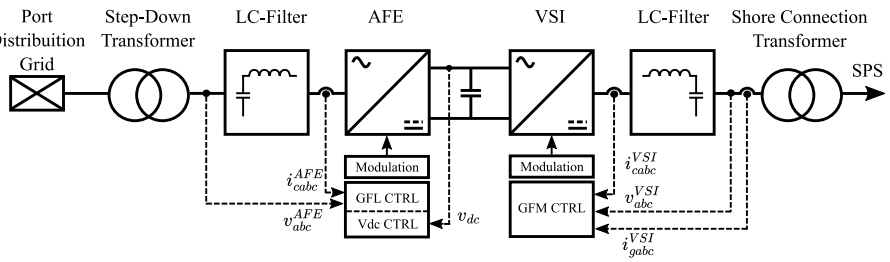

Fig. 4. HVSC One Line Diagram with Controls.

Table 3
Components used for the simulation of the different case studies.

Component #	Component name	Case study #1	Case study #2	Case study #3
1	Power system model	X	X	
2	RECs	X		
3	RT Forecasting tool			X
4	RT Charging Station Management			X
5	Measures from a real PV field	X	X	X
6	Port Electrification model		X	
7	Wind Farm with inertial controller	X	X	
8	Microgrid with Flexible DERs (in PHIL)	X	X	
9	Traditional MV Grid	X		X

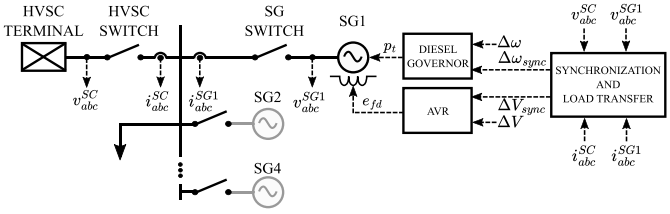

Fig. 5. SPS One Line Diagram with Controls.

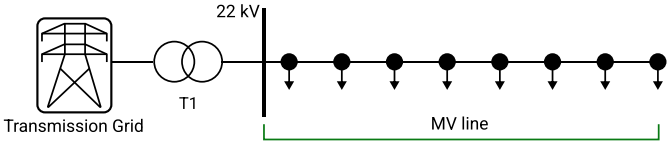

Fig. 6. Distribution grid.

transmission system thanks to their islanding capabilities. In order to properly assess the impact of the RECs at a system level, it is assumed that the grid has seen a large-scale roll-out of new communities. The simulations include 80 different communities, equally divided between the two types introduced in Section 3.2. The communities of type 1 have been simulated by running the model of a single community and by properly rescaling its power outputs. With this approach, the total power withdrawn from the grid in steady-state conditions amounts to 39.86 MW and 69.73 Mvar. A frequency-sensitive controller has been included to operate the circuit breakers of the RECs: the communities have the capability of disconnecting from the main network in case of frequency events (to mitigate frequency transients in the main grid) while continuing to operate in islanded mode. In the implemented logic, the RECs are disconnected when the network frequency reaches the critical value of 49.5 Hz and are reconnected back after the frequency is restored to at least 49.95 Hz. The same approach of power rescaling and frequency-driven disconnections has been adopted for the RECs of type 2. In this case, the steady-state power withdraw of the RECs amounts to 0.1 MW and 18.5 Mvar, thus characterized by limited frequency regulation capabilities. Nevertheless, the RECs are still capable of disconnecting from the main grid and operating in islanded mode to preserve the power supply to their members in scenarios where the main network frequency reaches critical values. In order to distinguish the behavior and impact of the two types of REC in case of frequency event, a slightly different disconnection logic is implemented for the RECs of type 2, maintaining the a disconnection frequency threshold of 49.5 Hz while considering a reconnection value of 49.92 Hz.

4.1.1. *GD-RTS implementation*

The models of the transmission network and of the different distribution elements have been connected with an asynchronous Alternate Current (AC) coupling using an Ideal Transformer Model (ITM), as described for example in [32]. The voltage signals (in terms of amplitude and frequency) measured in the transmission network at the points of connection are exchanged and used in the simulation of the different distribution elements. In turn, the active and reactive power measured at the points of connection at the distribution level are sent to the transmission network, where they are considered as parameters of PQ dynamic loads.

4.1.2. *Simulation results*

The simulated scenario considers an emergency condition in the transmission network arising from the abrupt equivalent load increase of 250 MW, i.e. about 17% of the entire system load, which occurs on bus 2 at time $t = 20.32$ s of the simulation time horizon. The frequency values measured at different points of the analyzed network are represented in Fig. 8.

As expected, there is a sharp decrease of the network frequency signal (exacerbated by the low inertia of the system) following the load increase. It is worth noting that the frequency values measured at the different buses are more or less equal, with one significant exception, i.e., the purple trace associated to the frequency in the RECs of type 1. Consistently with the implemented control logic, these RECs are disconnected from the main grid once the network frequency goes below the threshold value of 49.5 Hz (t =22 s). At this stage, the RECs operate in islanded mode relying exclusively on their local generation assets, preserving the power supply to their members and, at the same time, contributing to support the frequency recovery by reducing the aggregate load demand by 39.86 MW. Note that, following the disconnection, the REC frequency exhibits a positive spike, due to the limited inertia of the REC and the aggressive control actions required to transition to islanded operation. Nevertheless, the frequency remains well within the boundary of a 0.5 Hz deviation from the nominal

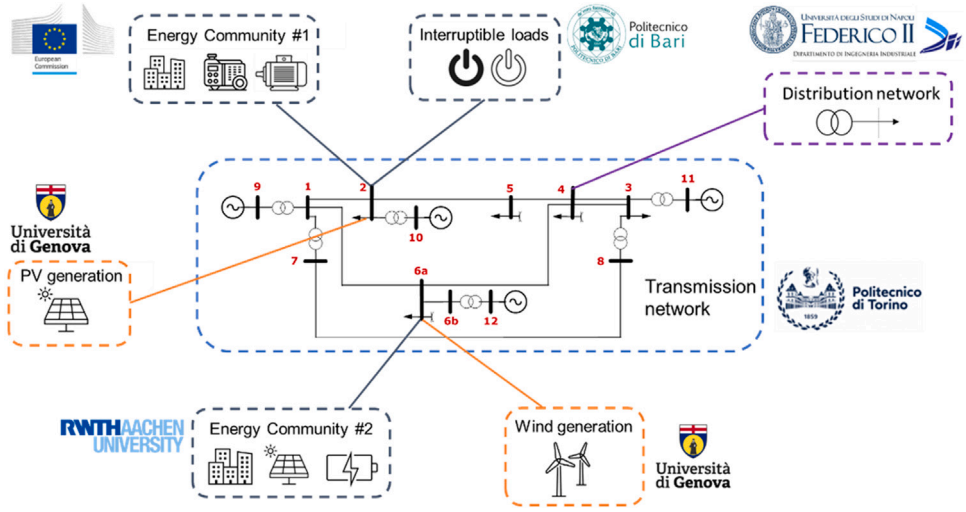

Fig. 7. Co-simulation layout.

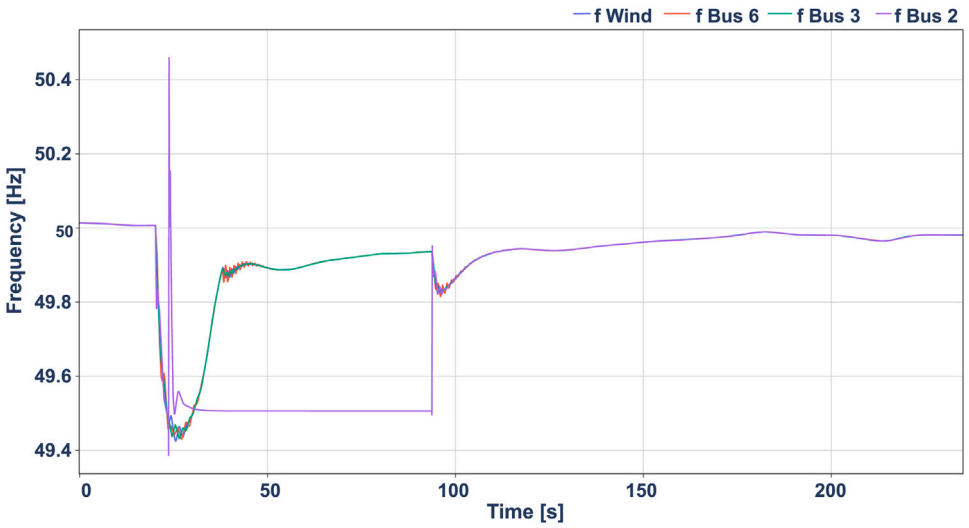

Fig. 8. Network frequency at the different network buses. (For interpretation of the references to color in this figure legend, the reader is referred to the web version of this article).

value, consistently with the prescribed frequency threshold value of 49.5 Hz considered for the REC disconnection. Once the frequency in the grid is restored to a threshold value of 49.95 Hz (t = 93 s), the RECs are reconnected and synchronized with the main grid. The synchronization of the REC is carried out with a $\Delta f \approx 0.5$ Hz, due to the limited amount of REC generation resources that do not permit to re-establish frequency value closer to the nominal one. This represents a challenging situation and, at the same time, enables to show that the reconnection is in any case successfully performed without endangering the stability of the system. The resulting load increase in the system causes a small frequency reduction that is quickly compensated by the secondary frequency regulation of the network.

The contribution of the different grid elements to the frequency regulation of the grid can be ascertained from Figs. 9 and 10, which show the power generation of the connected renewable sources and the power consumption of the connected loads and RECs, respectively. From Fig. 9, it can be seen how the PV generation installed at bus 2 (red trace) does not provide any type of frequency support and maintains a constant power generation of about 25 MW. Conversely, the inertial controller of the wind farm at bus 6 (whose generation profile is depicted in blue) is able to actively provide frequency support by releasing part of the kinetic energy stored in the rotating shafts of the wind turbines. If one considers the load profiles shown in Fig. 10, it can be seen how, consistently with the frequency behavior discussed in Fig. 8, the power absorbed from the grid by the RECs of type 1 (green trace) goes to zero once these are disconnected from the network because of critical frequency values (below 49.5 Hz) and it quickly returns to its initial value once safer frequency values (above 49.95 Hz) are reached and the RECs are reconnected to the grid. Similarly, the disconnection (and subsequent reconnection) of the 35 MW interruptible load, which is connected at bus 6, can be noticed in the lower values of the orange trace between t = 25 s and t = 40 s. Finally, in the case of the distribution grid connected at bus 4 (blue trace), no specific control action is taken and the absorbed power remains approximately equal to about 35 MW during the whole simulation.

4.2. Case study #2: impact of port electrification on power system

Fig. 11 shows the layout of the case study assessing the ship connection and disconnection. Fig. 12 illustrates an example of a cruise connection to the HVSC terminals. At t = 0 s the ship is disconnected from the HVSC. The SG supplies the ship load, the SG switch is closed and the HVSC switch is open. At t = 3 s (dotted blue line), the SG initiates synchronization with the HVSC voltage. By t = 3.5 s (dotted

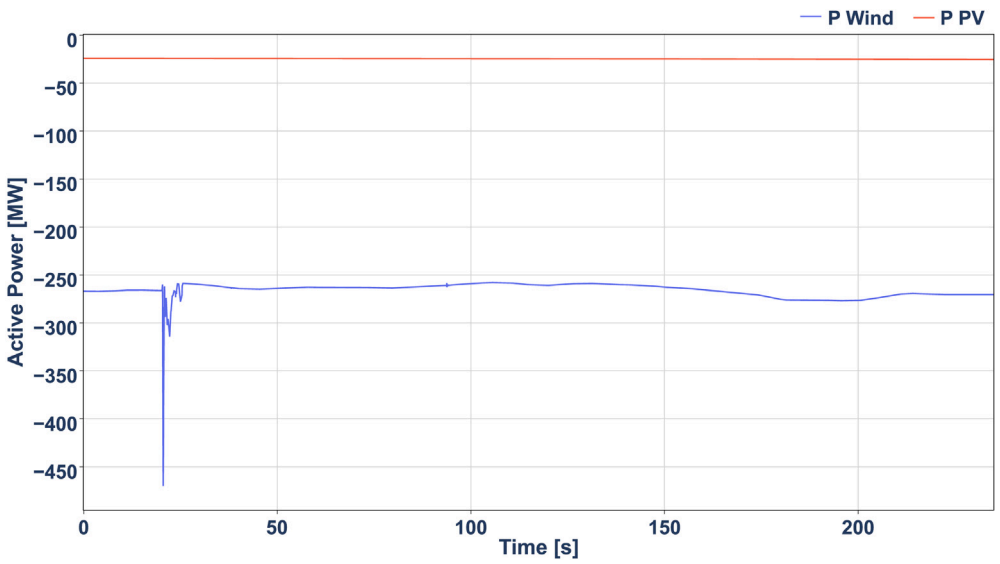

Fig. 9. Power generation of the connected renewable sources. (For interpretation of the references to color in this figure legend, the reader is referred to the web version of this article).

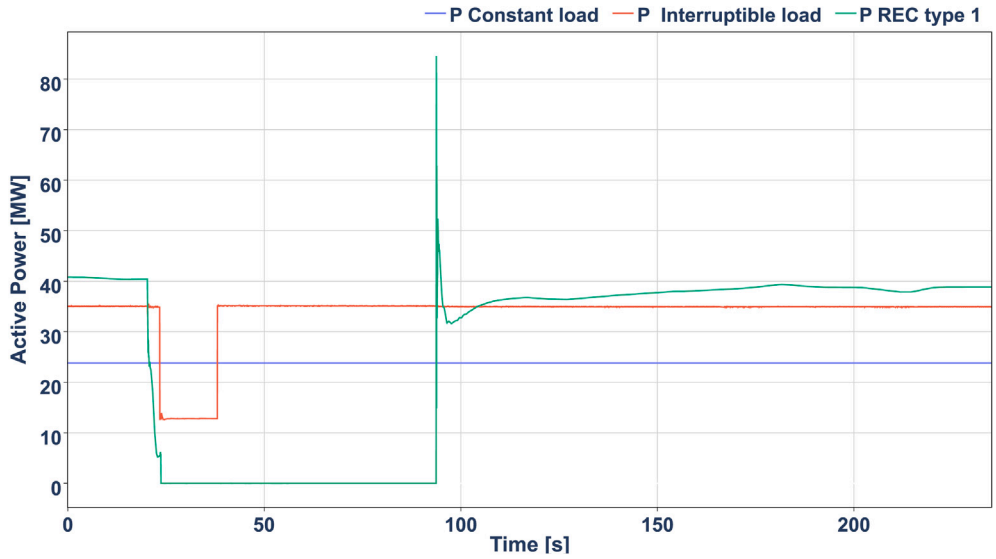

Fig. 10. Power consumption of the connected loads and renewable energy communities.

red line), the synchronization conditions are satisfied, leading to the closing of the HVSC switch. From $t = 3.5$ s to $t = 15.1$ s (dotted green line), power is transferred from the SG to the HVSC. At $t = 15.1$ s, the power flowing into the SG switch reaches zero. Consequently, the SG switch opens, allowing the SG to be turned off. The case study involves a notional port with multiple HVSC terminals and an aggregated port load. Each HVSC terminal is equipped with its own static converter and insulation transformer. The model includes high detail components such as the static converter and its control system, the SPS automation for connecting to the HVSC, the SG and its control system. In this scenario, one Cruise ship, one Ferry and one refrigerated cargo ship (Reefer) have the capability to connect and disconnect from their respective HVSC terminals. Table 4 provides details on the power requirements of the ships when berthed, along with their rated voltage and frequency. The case study aims to highlight the importance of coordination between the port microgrid operator and the DSO during the connection of ships. The critical events in this study involve the rapid connection and disconnection of multiple ships. Fig. 13 depicts the active power demand from both the port and the HVSC terminals. It illustrates the sequential connection of the Cruise ship, followed by the Ferry after a 3 s interval, and a container ship with Reefer after an additional 3 s. As the three ships link to the shore, the port active demand increases from 11 MW to 35 MW. Consequently, the grid frequency drops to a nadir of 49.96 Hz. Fig. 14 depicts the active power demand from the port and the HVSC terminals. It illustrates the disconnection of the Cruise ship, the Ferry, and the Reefer ships with a delay of 3 s among them. When the three ships disconnect from the shore, the port's active demand decreases from 35 MW to 11 MW. As a result, the grid frequency rises to a maximum of 50.047 Hz. Both the connection and disconnection of ships have the potential to induce hazardous frequency deviations if carried out without proper coordination. Therefore, it is imperative that future ports implement a coordinated approach with the grid operator for ship connections and disconnections to effectively mitigate these risks. As final remarks regarding this case, the simulated HVSC facilities comply with the IEEE 80005 [57] standard and can be scaled as needed in terms of nominal power. The converters and controller technologies are perfectly aligned with the ones commercially available today. The ship grid models are

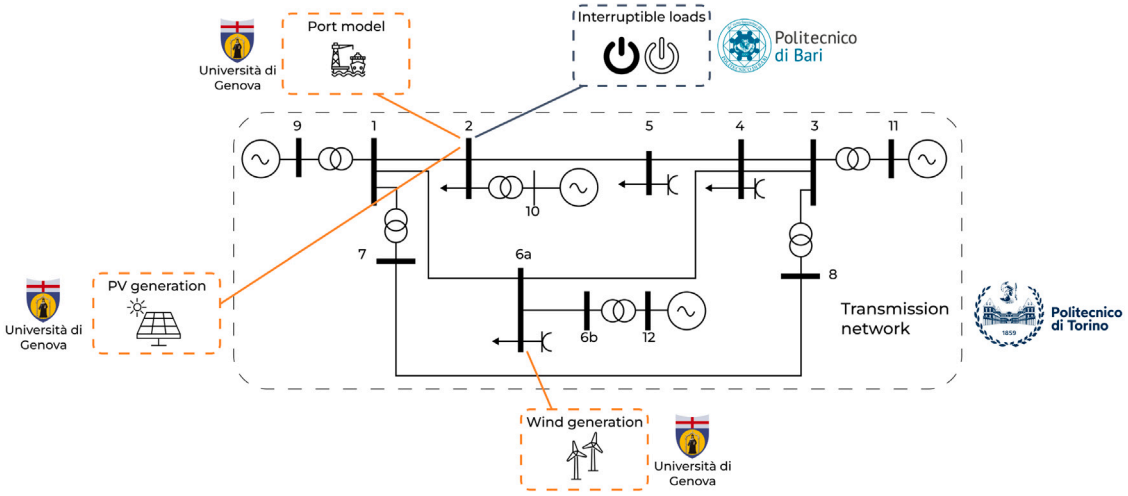

Fig. 11. Co-simulation layout case 2.

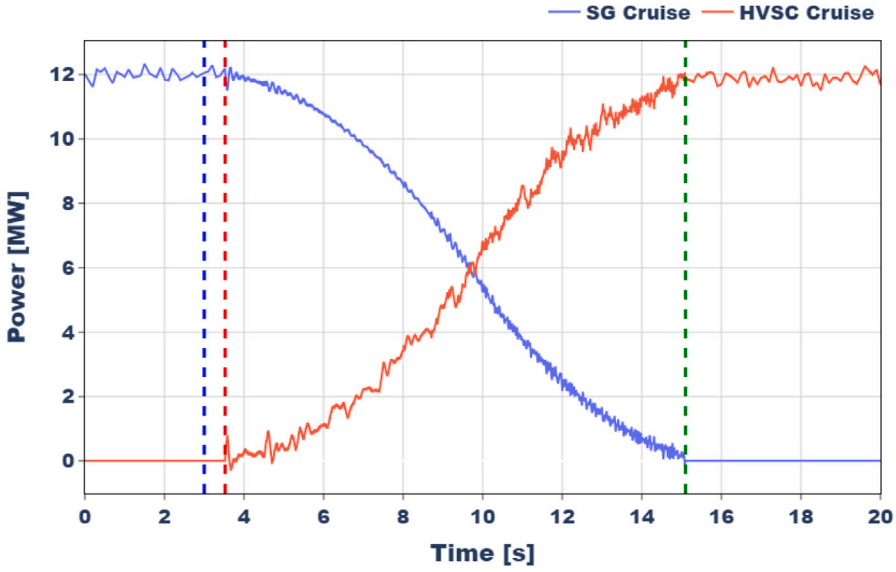

Fig. 12. Cruise Berth Connection Power Transfer. (For interpretation of the references to color in this figure legend, the reader is referred to the web version of this article).

Table 4
Ships power demand at berth.

Ship Type	Rated Voltage	Rated Frequency	Berthed Power
Cruise	11 kV	60 Hz	12 MW
Ferry	11 kV	60 Hz	6 MW
Reefer	11 kV	60 Hz	6 MW

also scalable in terms of synchronous generators nominal power. Thus, the port model can be adjusted for any port load power, number of HVSC connections, and load port power demand.

4.3. Case study #3: management of EV charging with forecasting tools

For this case study, a multi-step forecasting framework has been developed to predict the PV solar generation profile on the basis of historical data. Fig. 15 shows the co-simulation layout of the implemented setup. The GD-RTS approach is important here because it enables, in the real world, to keep confidential the developed algorithm during the test phase. The model f_h introduced in Section 3.3.3 is trained offline using as set an exclusive portion of the available data, whereas the rest acts as an unforeseen dataset for the validation stage. This direct strategy has been used because it is usually less prone to accumulated error with respect to alternative iterative strategies, where only one model is built and the forecasting samples will be used as input for the next step ahead over the forecasting horizon span at the same time step t. However, one of the drawbacks is the potential lack of correlation between the prediction of the consecutive time step over the forecasting horizon span [63].

In order to address this task considering the PV power generation as the only available time-series, the Support Vector Machine (SVM) regression has been considered as a suitable model. It is important to note that this case study aims to show how a regression model could be integrated into a co-simulation platform (i.e., proposing an innovative forecasting methodology is beyond the scope).

The training of the models is performed offline, where the input is the past samples according to a set of lag loop-back values $L = \{1, \ldots, 15\}$, whereas $H = \{1, \ldots, 5\}$. The time resolution of data is 1 minute: this means that the framework will predict the future PV power generation profiles for the next 5 min. The period covered by the available data is 10 days, with a ratio between training/test ratio of 0.9/0.1. Data are arranged according to H and L sets using an embedding procedure. This means that the last day was used to test the prediction accuracy. Once the models are trained, they

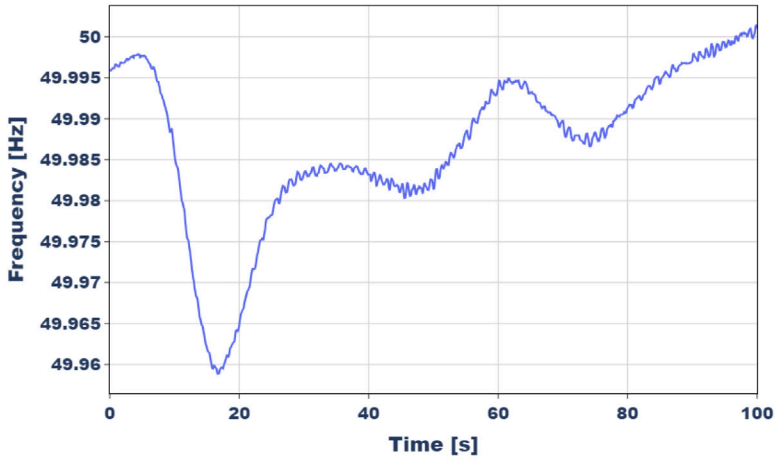

(a) Inland Grid Frequency

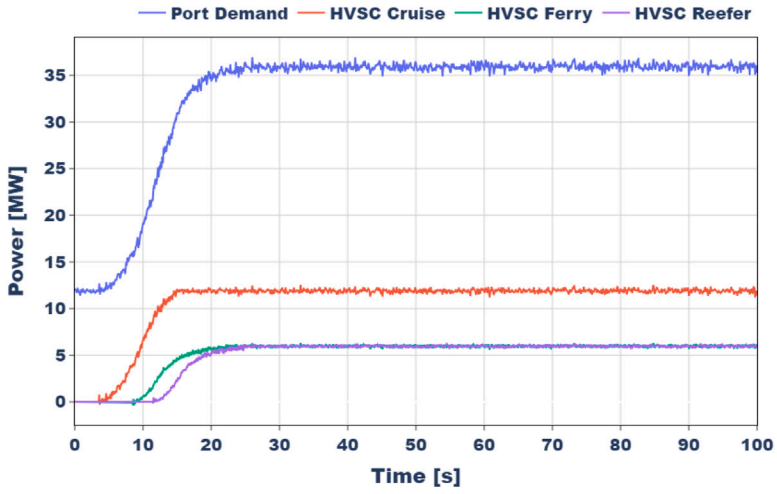

(b) Power Demands

Fig. 13. Connection of Multiple Ships to the Port.

are ready to be loaded in the co-simulation model. In particular, Fig. 16 shows a picture of the Simulink model loaded in the real-time simulator.

The acquisition and elaboration of the input/actual data are emulated through block set A, where the top block (A1) processes input data, whereas the bottom block (A2) is included in the current version of the project only for testing purposes and does not affect the Multi-Step Ahead Forecasting model block. Block B performs the PV forecasting, where five models return the forecast values since a direct multi-step strategy has been applied. Hence, the data are collected and sent to Block set C for making the output dimensional. Once the future PV generation samples are predicted, they are merged in a signal vector and passed to the unscaler. When the PV generation multi-step predictions take the original dimensions, they are shared via Villas to the RT Charging Station Management system. In Fig. 17, four out of five of the predicted future samples are compared with the real PV production. Finally, thanks to the forecast signals, the optimization described in Section 3.4 has been run, obtaining the power setting to be sent to the EVSEs, resulting in the power and SoC profiles shown in Fig. 18 and Fig. 19. The presented results cover only a part of the day, because of the long time needed to carry out the experiment in RT (this aspect still persists even speeding up the simulation, i.e., sending the needed signals more frequently to emulate a faster time step). The results presented in Figs. 18 and 19 are directly linked to the optimization framework presented as Component #4 in Section 3.4. Specifically, the predictive models have yielded results consistent with the expected outcomes based on the theoretical framework, as in constraints shown in Eq. (5) and in Eqs. from (9) to (12). This alignment confirms the robustness of our approach, where the forecasting tool significantly contributes to optimize the charging station management by predicting solar generation.

Regarding this case study, in the forecasting model the developed SVM-based forecaster can be easily replaced with other offline-trained models, where the only requirement is to preserve the exact input and output variables. Changes will require adapting some settings in blocks A1/A2 and slight changes in block B of Fig. 16, especially if it will be necessary to change the forecasting horizon. Finally, the computational demand is not a problem since the model is already trained. The optimization component should not have any relevant issues regarding its replicability in other experimental setups as well. In fact, the management system of the chargers is implemented as separate component that communicates with the simulated environment as described in Section 3.4.

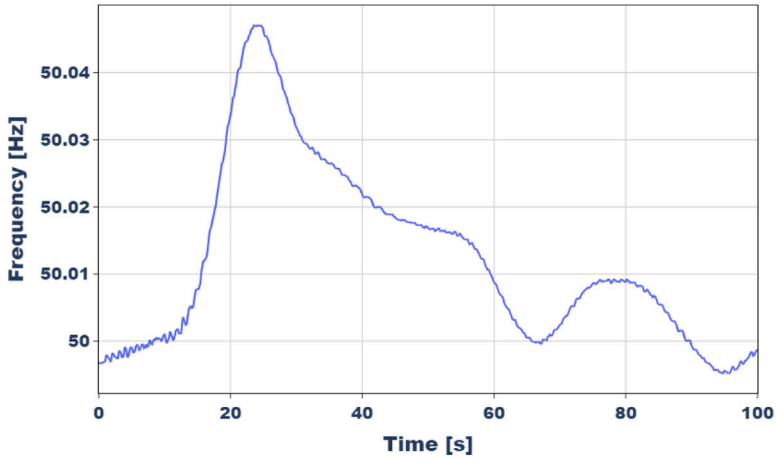

(a) Inland Grid Frequency

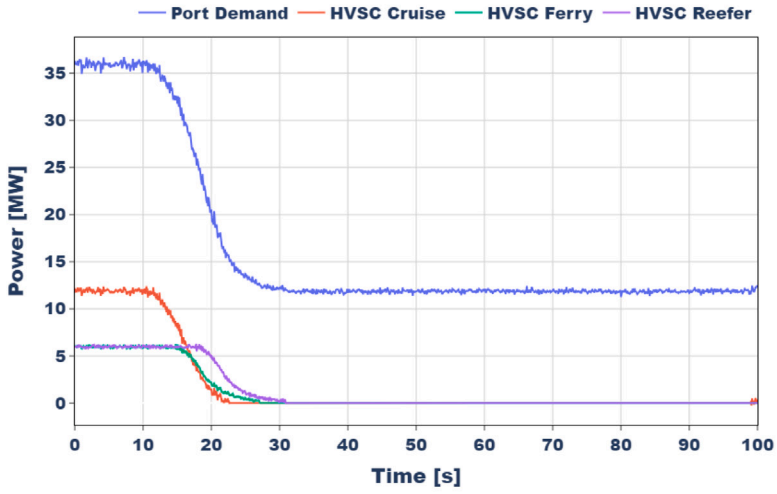

(b) Power Demands

Fig. 14. Disconnection of Multiple Ships from the Port.

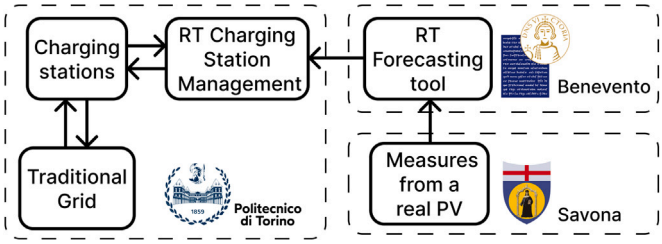

Fig. 15. Co-simulation layout case study 3.

5. Lessons learnt: discussion about practical implementation aspects

This section summarizes the lessons learnt from setting up the mentioned GD-RTS collaboration platform, trying to emphasize limitations and problems that may be experienced when replicating it:

- The very first and time-consuming step was the setting of the connections among different laboratories and institutions. In fact, every partner employs different RTS technologies; moreover, the ICT department of the different institutions manage differently the internet network through several approaches to control the in/out data traffic. Some of the involved institutions require high standards in terms of cyber-security and keep their system behind secure firewalls. The adoption of Virtual Power Network (VPN) tunnels (with an IPSec encryption to protect data) was a solution acceptable by all the involved parties. Although configuring and establishing a VPN tunnel is a very standard procedure for any ICT administrator, this procedure requires fine tuning among all participating parties, which have to adopt the same protocols, establishing the rules of communication and find common domains to operate. Hence, each connection required a customization.
- Since IP-based communication was adopted, even the management of assigned IPs and domains was problematic. In fact, some institutions use public IPs, which are unique, but other employ IPs within the private address range. Finding domains which are not already assigned in multiple private networks can be a hard task with two institutions, and becomes practically impossible with several ones. Translation of IPs through Network Address Translation (NAT) is clearly possible, but this is again a procedure requiring customization and multiple time-consuming iterations among the parties.
- Once established a connection, each link of the GD-RTS platform was tested in order to assess its performances in terms of quality and speed. In general, no specific problems were observed,

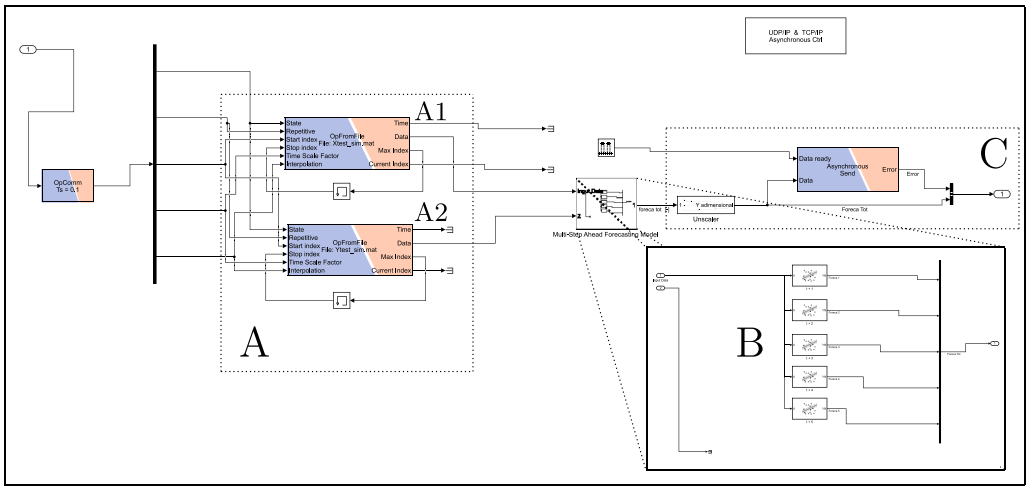

Fig. 16. PV forecasting architecture in Simulink.

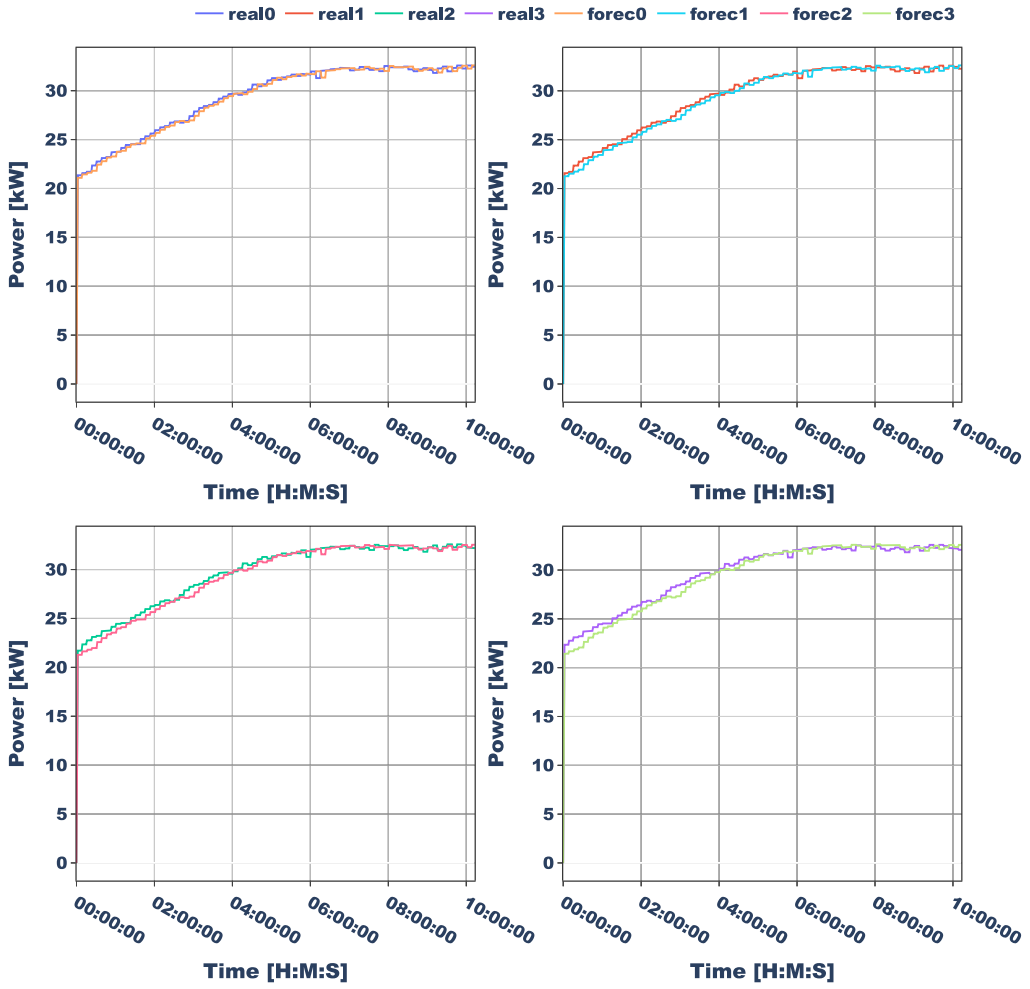

Fig. 17. Forecasted signal.

although each communication was characterized by a different delay due to the physical distance between the nodes. Delays and lost packets by employing User Datagram Protocol (UDP) protocol were rigorously studied in [64] for the connection with the longest distance (i.e., Bari-Torino, almost 1,000 km). Thanks to the adoption of the public GARR network and to the use of the UDP protocol, the speed of communication was assessed in about 12–12.5 ms that is about one quarter of the ideal time required by light to run the same distance. Average delay can be contained sending UDP packets with a rate higher than the sampling rate of the exchanged data. This means that the same datum is sent multiple times, by increasing the probability of being received. The UDP protocol enables the rejection of the delayed packets and keeps the last ones: in this way, the delays can be abated

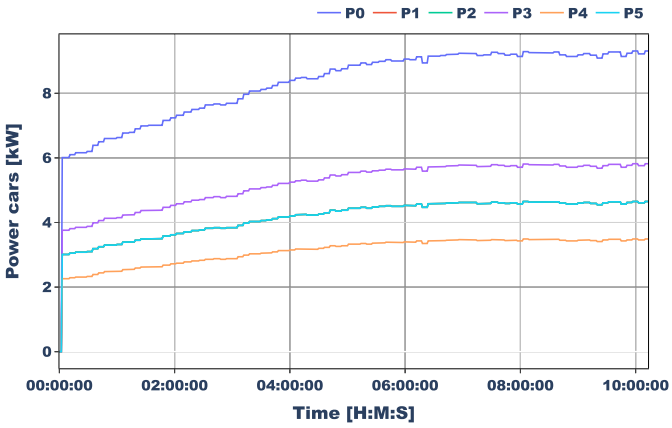

Fig. 18. Power sent to the cars.

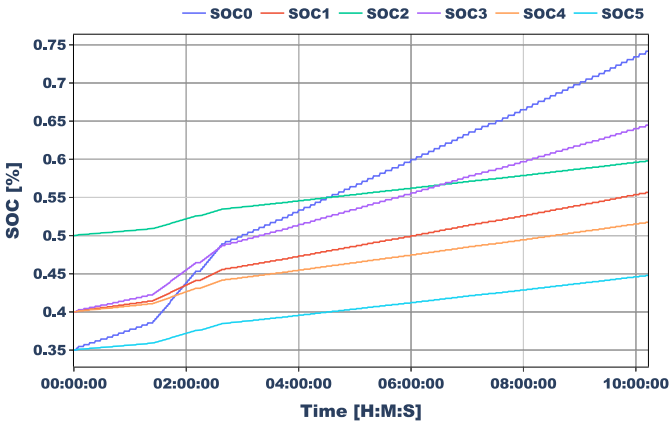

Fig. 19. Measured SOC of the cars.

although some packets may be lost [64]. This is not a problem, because each packet is re-transmitted with a high transmission rate (usually one packet every 1 or 2 ms).

- Multiple technologies were adopted in this study. GD-RTS included different brands (OPAL-RT, RTDS, Speedgoat); moreover, several hardware components were interfaced through Modbus TCP/IP and other communication protocols. Interfacing different brands of RT simulators can be problematic since, datagrams can be built with different structures, even when they use the same protocol. A "translator" is usually needed as middleware between all RT systems. In this implementation, the VILLAS Framework is used to translate and redirect all communications. Given the structure of the GD-RTS platform, built using a start topology around PoliTO's node, the VILLAS Node in Torino was used as a (master) hub to collect all data and manage connections.
- The star structure of the communication is coherent with the co-simulation model: in fact, the model was built around a transmission system (i.e., simulated by PoliTo as main electrical infrastructure), connected to other sub-systems set on lower voltage level (corresponding to the other nodes). The adoption of an ITM for coupling these nodes permitted to synchronize all co-simulations with the master simulation and achieve stability, even in presence of different communication delays.
- It is worth noting that, as proven in [61], ITM guarantees stability before accuracy. Accuracy of co-simulation can be affected by delays, especially in the presence of very fast controllers. For example, some additional GD-RTS experimental tests involving the adoption of synthetic inertia controllers at a high geographical distance, were characterized by the on-set of low-frequency oscillations due to the delays in the co-simulation rather than to some physical phenomena. This is an important issues because it must be stressed out that RT co-simulation cannot have one structure that fits all. Each experiment requires careful planning, an assessment of the needed resources, and must handle with delays and other physical constraints.
- Co-simulations involving Power Hardware-in-the-Loop (PHIL) equipment raise relevant security concerns: they must be carefully orchestrated and require the physical presence and time availability of all the people involved.

6. Concluding remarks

This work focused on the application of GD-RTS for exploring different aspects of the energy transition. Particularly, the GD-RTS platform can operate at a continental scale by sharing simulation resources of seven RTS laboratories (one located in Germany and six located across the Italian peninsula), integrating the cyber and/or physical response of their equipment in the same simulation environment. Sharing research infrastructure and resources is essential to achieve a realistic representation of complex cyber–physical systems where multiple grids, subsystems, controllers, and power devices must interact. In particular, we considered nine different components (SIL, PHIL and HIL), each managed by one of the laboratories involved into the co-simulation. These components have been combined to create three distinct case studies, analyzing some of the most relevant scenarios in future decarbonized power systems. These have included: (*i*) the operation of low-inertia power system thanks to new resources and control approaches, (*ii*) integration of electrified port facilities within the power network, and (*iii*) the operation of a parking lot combining PV forecasting and charging station operation, both running in RT.

The proposed case studies represent an advanced investigation of the capabilities offered by the GD-RTS for planning and managing complex energy systems endowed with different types of assets and technologies. The use of a real-time approach has enabled the direct integration of hardware and software components in the simulation environment, achieving improved accuracy and robustness. In parallel, the Geographically-Distributed implementation of the studies has allowed to pool the expertise and resources of several laboratories and research groups, developing multi-disciplinary case studies of relevant interest and significance.

Future work will focus on the extension of the developed simulation framework through the inclusion of additional laboratories. The final objectives in this regard are the creation of a large network of interconnected simulation facilities, the standardization of the connection procedures, the creation of a meshed configuration to improve the co-simulation flexibility and the development of a comprehensive set of representative benchmarks systems, to be tuned on an *ad-hoc* basis for specific studies. Moreover, we will map the kind of GD-RTS tests that can be accomplished with our network, according to the distance of locations and software/hardware equipment availability.

CRediT authorship contribution statement

A. Mazza: Writing – review & editing, Writing – original draft, Supervision, Methodology, Formal analysis, Conceptualization. **G. Benedetto:** Writing – review & editing, Writing – original draft, Visualization, Software, Investigation. **E. Pons:** Writing – review & editing, Validation, Data curation. **E. Bompard:** Resources, Funding acquisition. **A. De Paola:** Writing – review & editing, Writing – original draft, Software, Methodology, Formal analysis, Conceptualization. **D. Thomas:** Validation, Data curation. **E. Kotsakis:** Validation, Data curation. **G. Fulli:** Resources, Funding acquisition. **S. Vogel:** Writing – original draft, Visualization. **A. Acosta Gil:** Writing – review & editing, Visualization. **A. Monti:** Resources, Funding acquisition. **S. Bruno:** Writing – review & editing, Writing – original draft, Supervision,

Methodology, Formal analysis, Conceptualization. **C. Iurlaro:** Writing – original draft, Visualization, Software, Investigation, Data curation. **M. La Scala:** Resources, Funding acquisition. **A. Bonfiglio:** Writing – original draft, Software, Methodology, Formal analysis, Data curation, Conceptualization. **P. Cepollini:** Writing – review & editing, Writing – original draft, Visualization, Software, Methodology, Investigation. **F. D'Agostino:** Writing – review & editing, Writing – original draft, Supervision, Software, Methodology, Conceptualization. **M. Invernizzi:** Resources, Funding acquisition. **M. Rossi:** Writing – review & editing, Writing – original draft, Visualization, Methodology, Investigation, Data curation. **F. Silvestro:** Resources, Funding acquisition. **F. De Caro:** Writing – review & editing, Writing – original draft, Visualization, Methodology, Investigation, Data curation. **G. Giannoccaro:** Writing – original draft, Visualization, Validation, Software, Investigation, Data curation. **D. Villacci:** Resources, Funding acquisition.

Declaration of competing interest

The authors declare that they have no known competing financial interests or personal relationships that could have appeared to influence the work reported in this paper.

Data availability

Data will be made available on request.

Acknowledgments

The project was supported by the National Recovery and Resilience Plan (NRRP), Mission 4 Component 2 Investment 1.3 - Call for Tender No. 341 dated 15.03.2022 of Ministero dell'Università e della Ricerca (MUR); funded by the European Union – NextGenerationEU. Project code PE0000021, Concession Decree no. 1561 of 11.10.2022 adopted by Ministero dell'Università e della Ricerca (MUR), CUP - D33C22001330002, D93C22000900001, E13C22001890001, E63C22 002160007 - Project title "Network 4 Energy Sustainable Transition – NEST".

References

[1] R. Pinto, et al., The rise and stall of world electricity efficiency: 1900–2017, results and insights for the renewables transition, Energy 269 (2023) 126775, http://dx.doi.org/10.1016/j.energy.2023.126775.

[2] G. Fridgen, R. Keller, M.-F. Körner, M. Schöpf, A holistic view on sector coupling, Energy Policy 147 (2020) 111913, http://dx.doi.org/10.1016/j.enpol.2020.111913.

[3] V. Heinisch, L. Göransson, R. Erlandsson, H. Hodel, F. Johnsson, M. Odenberger, Smart electric vehicle charging strategies for sectoral coupling in a city energy system, Appl. Energy 288 (2021) 116640, http://dx.doi.org/10.1016/j.apenergy.2021.116640.

[4] Directive (EU) 2018/2001 of the European Parliament and of the Council of 11 December 2018 on the promotion of the use of energy from renewable sources, OJ L 328 (2018) 82–209.

[5] RESCOOP.eu transposition tracker, 2024, https://www.rescoop.eu/policy/transposition-tracker. (Accessed: 26 April 2024).

[6] European Commission, Staff Working Document Impact Assessment Accompanying the Document Proposal for a Directive of the European Parliament and of the Council on the Promotion of the Use of Energy from Renewable Sources (Recast), Tech. Rep., 2016.

[7] A. Caramizaru, A. Uihlein, Energy Communities: An Overview of Energy and Social Innovation, Tech. Rep., Joint Research Centre, 2020.

[8] Z.A. Khan, D. Jayaweera, Smart meter data based load forecasting and demand side management in distribution networks with embedded PV systems, IEEE Access 8 (2020) 2631–2644, http://dx.doi.org/10.1109/ACCESS.2019.2962150.

[9] R. Trivedi, S. Patra, S. Khadem, A data-driven short-term PV generation and load forecasting approach for microgrid applications, IEEE J. Emerg. Sel. Top. Ind. Electron. 3 (4) (2022) 911–919, http://dx.doi.org/10.1109/JESTIE.2022.3179961.

[10] A. De Paola, D. Thomas, E. Kotsakis, G. Fulli, M. Lugano, D. Ferrero, S. Olivero, A predictive tool for techno-economical analyses of renewable energy communities, in: 2023 International Conference on Smart Energy Systems and Technologies, SEST, 2023, pp. 1–6, http://dx.doi.org/10.1109/SEST57387.2023.10257428.

[11] P. Scarabaggio, R. Carli, J. Jantzen, M. Dotoli, Stochastic model predictive control of community energy storage under high renewable penetration, in: 2021 29th Mediterranean Conference on Control and Automation, MED, 2021, pp. 973–978, http://dx.doi.org/10.1109/MED51440.2021.9480353.

[12] H. Zhu, K. Ouahada, A.M. Abu-Mahfouz, Peer-to-peer energy trading in smart energy communities: a Lyapunov-based energy control and trading system, IEEE Access 10 (2022) 42916–42932, http://dx.doi.org/10.1109/ACCESS.2022.3167828.

[13] D. Thomas, I. Kounelis, E. Kotsakis, A. De Paola, G. Fulli, Sharing unused storage in local energy markets utilizing physical storage rights: A non-cooperative game theoretic approach, J. Energy Storage 55 (2022) 105755, http://dx.doi.org/10.1016/j.est.2022.105755, URL https://www.sciencedirect.com/science/article/pii/S2352152X22017431.

[14] IEA, Energy system: transport, 2023, URL https://www.iea.org/energy-system/transport. (Access 11 January 2023).

[15] EN IEC 61851 - 1: Electric vehicle conductive charging system. General requirements, in: International Electrotechnical Commission, IEC, 2019.

[16] Voltage Characteristics of Electricity Supplied by Public Electricity Networks, British Standards Institution, 2010.

[17] M.A. Awadallah, B.N. Singh, B. Venkatesh, Impact of EV charger load on distribution network capacity: a case study in toronto, Can. J. Electr. Comput. Eng. 39 (4) (2016) 268–273, http://dx.doi.org/10.1109/CJECE.2016.2545925.

[18] T.M.H. Slangen, T. van Wijk, V. Ćuk, J.F.G. Cobben, The harmonic and supraharmonic emission of battery electric vehicles in The Netherlands, in: 2020 International Conference on Smart Energy Systems and Technologies, SEST, 2020, pp. 1–6, http://dx.doi.org/10.1109/SEST48500.2020.9203533.

[19] M.H.J. Bollen, M. Olofsson, A. Larsson, S.K. Ronnberg, M. Lundmark, Standards for supraharmonics (2 to 150 kHz), IEEE Electromagn. Compat. Mag. 3 (2014) 114–119.

[20] A. Lucas, F. Bonavitacola, E. Kotsakis, G. Fulli, Grid harmonic impact of multiple electric vehicle fast charging, Electr. Power Syst. Res. 127 (2015) 13–21, http://dx.doi.org/10.1016/j.epsr.2015.05.012.

[21] Directive 2014/94/EU: Regulation of the European Parliament and of the Council on the deployment of alternative fuels infrastructure, and repealing, (1804) 2023, pp. 1–144.

[22] F. D'Agostino, G.P. Schiapparelli, S. Dallas, D. Spathis, V. Georgiou, J. Prousalidis, On estimating the port power demands for cold ironing applications, in: 2021 IEEE Electric Ship Technologies Symposium, ESTS, 2021, pp. 1–5.

[23] H. Bevrani, H. Golpî ra, A.R. Messina, N. Hatziargyriou, F. Milano, T. Ise, Power system frequency control: An updated review of current solutions and new challenges, Electr. Power Syst. Res. 194 (2021).

[24] S.S. Guggilam, C. Zhao, E. Dall'Anese, Y.C. Chen, S.V. Dhople, Optimizing DER participation in inertial and primary-frequency response, IEEE Trans. Power Syst. 33 (5) (2018) 5194–5205.

[25] S. Bruno, G. Giannoccaro, C. Iurlaro, M. La Scala, C. Rodio, Power hardware-in-the-loop test of a low-cost synthetic inertia controller for battery energy storage system, Energies 15 (9) (2022) http://dx.doi.org/10.3390/en15093016.

[26] S. Bruno, G. Giannoccaro, C. Iurlaro, M.L. Scala, M. Menga, C. Rodio, R. Sbrizzai, Fast frequency support through LED street lighting in small non-synchronous power systems, IEEE Trans. Ind. Appl. 59 (2) (2023) 2277–2287.

[27] V. Prakash, H. Pandzic, Fast frequency control service provision from active neighborhoods: Opportunities and challenges, Electr. Power Syst. Res. 217 (2023) 109161.

[28] G. Benedetto, A. Mazza, E. Pons, E. Bompard, A. De Paola, D. Thomas, E. Kotsakis, G. Fulli, S. Vogel, A. Monti, S. Bruno, G. Giannoccaro, M.L. Scala, A. Bonfiglio, M. Invernizzi, M. Rossi, F. De Caro, D. Villacci, Supporting a 'glocal' energy transition: from local energy communities to global simulation networks, in: 2023 International Conference on Smart Energy Systems and Technologies, SEST 2023, 2023, http://dx.doi.org/10.1109/SEST57387.2023.10257451, URL https://www.scopus.com/inward/record.uri?eid=2-s2.0-85174247594&doi=10.1109%2fSEST57387.2023.10257451&partnerID=40&md5=3744e5d017e383349a6a0565f4b1e429.

[29] A. Benigni, T. Strasser, G. De Carne, M. Liserre, M. Cupelli, A. Monti, Real-time simulation-based testing of modern energy systems: a review and discussion, IEEE Ind. Electron. Mag. 14 (2) (2020) 28–39, http://dx.doi.org/10.1109/MIE.2019.2957996, Conference Name: IEEE Industrial Electronics Magazine, URL https://ieeexplore.ieee.org/abstract/document/9127176.

[30] M. Syed, et al., Applicability of geographically distributed simulations, IEEE Trans. Power Syst. 38 (4) (2023) 1–15, http://dx.doi.org/10.1109/TPWRS.2022.3197635.

[31] M. Stevic, S. Vogel, A. Monti, S. D'Arco, Feasibility of geographically distributed real-time simulation of HVDC system interconnected with AC networks, in: 2015 IEEE Eindhoven PowerTech, 2015, pp. 1–5, http://dx.doi.org/10.1109/PTC.2015.7232700, URL https://ieeexplore.ieee.org/abstract/document/7232700.

[32] M.H. Syed, et al., Real-time coupling of geographically distributed research infrastructures: taxonomy, overview, and real-world smart grid applications, IEEE Trans. Sm. Grid 12 (2) (2021) 1747–1760, http://dx.doi.org/10.1109/TSG.2020.3033070.

[33] B. Palmintier, D. Krishnamurthy, P. Top, S. Smith, J. Daily, J. Fuller, Design of the HELICS high-performance transmission-distribution-communication-market co-simulation framework, in: 2017 Workshop on Modeling and Simulation of Cyber-Physical Energy Systems, MSCPES, 2017, pp. 1–6, http://dx.doi.org/10.1109/MSCPES.2017.8064542, URL https://ieeexplore.ieee.org/abstract/document/8064542.

[34] E. Guillo-Sansano, M. H. Syed, A. J. Roscoe, G. M. Burt, Initialization and synchronization of power hardware-in-the-loop simulations: a great britain network case study, Energies 11 (5) (2018) http://dx.doi.org/10.3390/en11051087, URL https://www.mdpi.com/1996-1073/11/5/1087.

[35] G. Benedetto, et al., Ensiel national energy transition real time lab: a novel tool to shape the future energy system, in: 2022 AEIT International Annual Conference, AEIT, 2022, pp. 1–6, http://dx.doi.org/10.23919/AEIT56783.2022.9951729.

[36] M. Maniatopoulos, D. Lagos, P. Kotsampopoulos, N. Hatziargyriou, Combined control and power hardware in-the-loop simulation for testing smart grid control algorithms, IET Gener. Transm. Distrib. 11 (12) (2017) 3009–3018, http://dx.doi.org/10.1049/iet-gtd.2016.1341.

[37] Y. Wang, et al., A distributed control scheme of microgrids in energy internet paradigm and its multisite implementation, IEEE Trans. Ind. Inform. 17 (2) (2021) 1141–1153, http://dx.doi.org/10.1109/TII.2020.2976830.

[38] N. Kumar, S.K. Panda, Smart high power charging networks and optimal control mechanism for electric ships, IEEE Trans. Ind. Inform. 19 (2) (2023) 1476–1483, http://dx.doi.org/10.1109/TII.2022.3170484.

[39] N. Kumar, S.K. Panda, A multipurpose and power quality improved electric vessels charging station for the seaports, IEEE Trans. Ind. Inform. 19 (3) (2023) 3254–3261, http://dx.doi.org/10.1109/TII.2022.3170424.

[40] J. Kumar, M. Mekkanen, M. Karimi, K. Kauhaniemi, Hardware-in-the-loop testing of a battery energy storage controller for harbour area smart grid: A case study for Vaasa harbour grid, Energy Rep. 9 (2023) 447–454, http://dx.doi.org/10.1016/j.egyr.2023.01.068, 2022 The 3rd International Conference on Power, Energy and Electrical Engineering, URL https://www.sciencedirect.com/science/article/pii/S2352484723000720.

[41] J. Zelic, L. Novakovic, I. Klindo, G. Gruosso, Hardware in the loop framework for analysis of impact of electrical vehicle charging devices on distribution network, in: 2020 IEEE Vehicle Power and Propulsion Conference, VPPC, 2020, pp. 1–5, http://dx.doi.org/10.1109/VPPC49601.2020.9330863.

[42] A. Mazza, G. Benedetto, E. Bompard, C. Nobile, E. Pons, P. Tosco, M. Zampolli, R. Jaboeuf, Interaction among multiple electric vehicle chargers: measurements on harmonics and power quality issues, Energies 16 (20) (2023) http://dx.doi.org/10.3390/en16207051, URL https://www.mdpi.com/1996-1073/16/20/7051.

[43] E. Ucer, M.J. Kisacikoglu, Design and implementation of a hardware test-bed for real-time EV-grid integration analysis, in: 2022 IEEE Energy Conversion Congress and Exposition, ECCE, 2022, pp. 1–8, http://dx.doi.org/10.1109/ECCE50734.2022.9947704.

[44] E. Ucer, M. Kisacikoglu, Development of a hardware-in-the-loop testbed for a decentralized, data-driven electric vehicle charging control algorithm, IEEE Trans. Ind. Appl. (2024) http://dx.doi.org/10.1109/tia.2024.3384480.

[45] I. Jayawardana, C.N.M. Ho, Y. Zhang, A comprehensive study and validation of a power-HIL testbed for evaluating grid-connected EV chargers, IEEE J. Emerg. Sel. Top. Power Electron. 10 (2) (2022) 2395–2410, http://dx.doi.org/10.1109/JESTPE.2021.3093303.

[46] M. Restrepo, J. Morris, M. Kazerani, C.A. Cañizares, Modeling and testing of a bidirectional smart charger for distribution system EV integration, IEEE Trans. Smart Grid 9 (1) (2018) 152–162, http://dx.doi.org/10.1109/TSG.2016.2547178.

[47] M. Galici, M. Mureddu, E. Ghiani, F. Pilo, Blockchain-based hardware-in-the-loop simulation of a decentralized controller for local energy communities, Energies 15 (20) (2022) http://dx.doi.org/10.3390/en15207623.

[48] D. Stahleder, D. Reihs, F. Lehfuss, LabLink – A novel co-simulation tool for the evaluation of large scale EV penetration focusing on local energy communities, in: CIRED 2018 Ljubljana Workshop, 2018.

[49] D. Carta, et al., VILLASnode-based co-simulation of local energy communities, in: 2022 Open Source Modelling and Simulation of Energy Systems, OSMSES, 2022, http://dx.doi.org/10.1109/OSMSES54027.2022.9768933.

[50] A. Benigni, A. Xhonneux, D. Carta, T. Pesch, D. Muller, On the development of control solutions for local energy communities: An incremental prototyping approach and related infrastructure, at - Automatisierungstechnik 70 (12) (2022) 1095–1115, http://dx.doi.org/10.1515/auto-2022-0034, Publisher: De Gruyter (O), URL https://www.degruyter.com/document/doi/10.1515/auto-2022-0034/html.

[51] S. Vogel, M. Mirz, L. Razik, A. Monti, An open solution for next-generation real-time power system simulation, in: 2017 IEEE Conference on Energy Internet and Energy System Integration, EI2, 2017, pp. 1–6, http://dx.doi.org/10.1109/EI2.2017.8245739.

[52] CIGRE, Benchmark systems for network integration of renewable and distributed energy resources, 2014.

[53] R. Salcedo, et al., Banshee distribution network benchmark and prototyping platform for hardware-in-the-loop integration of microgrid and device controllers, J. Eng. 2019 (8) (2019) 5365–5373, http://dx.doi.org/10.1049/joe.2018.5174, arXiv:https://ietresearch.onlinelibrary.wiley.com/doi/pdf/10.1049/joe.2018.5174, URL https://ietresearch.onlinelibrary.wiley.com/doi/abs/10.1049/joe.2018.5174.

[54] F. De Caro, A. Andreotti, R. Araneo, M. Panella, A. Vaccaro, D. Villacci, A review of the enabling methodologies for knowledge discovery from smart grids data, in: Proceedings - 2020 IEEE International Conference on Environment and Electrical Engineering and 2020 IEEE Industrial and Commercial Power Systems Europe, EEEIC / I and CPS Europe 2020, 2020, http://dx.doi.org/10.1109/EEEIC/ICPSEurope49358.2020.9160678.

[55] R.E. Edwards, J. New, L.E. Parker, B. Cui, J. Dong, Constructing large scale surrogate models from big data and artificial intelligence, Appl. Energy 202 (2017) 685–699.

[56] F. De Caro, J. De Stefani, G. Bontempi, A. Vaccaro, D. Villacci, Robust assessment of short-term wind power forecasting models on multiple time horizons, Technol. Econ. Smart Grids Sustain. Energy 5 (2020) 1–15.

[57] IEC/IEEE 80005-1: Utility connections in port – High voltage shore connection (HVSC) systems – General requirements, 2019.

[58] R. Smolenski, G. Benysek, M. Malinowski, M. Sedlak, S. Stynski, M. Jasinski, Ship-to-shore versus shore-to-ship synchronization strategy, IEEE Trans. Energy Convers. 33 (4) (2018) 1787–1796.

[59] A. Bonfiglio, M. Invernizzi, A. Labella, R. Procopio, Design and implementation of a variable synthetic inertia controller for wind turbine generators, IEEE Trans. Power Syst. 34 (1) (2019) 754–764, http://dx.doi.org/10.1109/TPWRS.2018.2865958.

[60] S. Bruno, G. Giannoccaro, M. Muzammal Islam, C. Iurlaro, M. La Scala, M. Menga, C. Rodio, Control and Power Hardware-in-the-Loop tests for low-inertia power systems, in: 2022 AEIT International Annual Conference, AEIT, 2022, pp. 1–6, http://dx.doi.org/10.23919/AEIT56783.2022.9951753.

[61] E. Bompard, et al., Latency and simulation stability in a remote power hardware-in-the-loop cosimulation testbed, IEEE Trans. Ind. Appl. 57 (4) (2021) 3463–3473, http://dx.doi.org/10.1109/TIA.2021.3082506.

[62] G. Benedetto, E. Bompard, A. Mazza, E. Pons, R. Jaboeuf, P. Tosco, M. Zampolli, Impact of bidirectional EV charging stations on a distribution network: a Power Hardware-In-the-Loop implementation, Sustain. Energy Grids Netw. 35 (2023) 101106, http://dx.doi.org/10.1016/j.segan.2023.101106, URL https://www.sciencedirect.com/science/article/pii/S2352467723001145.

[63] G. Bontempi, S. Ben Taieb, Y.-A. Le Borgne, Machine learning strategies for time series forecasting, in: Business Intelligence: Second European Summer School, eBISS 2012, Brussels, Belgium, July 15-21, 2012, Tutorial Lectures 2, Springer, 2013, pp. 62–77.

[64] E. Bompard, S. Bruno, S. Frittoli, G. Giannoccaro, M.L. Scala, A. Mazza, E. Pons, C. Rodio, Remote PHIL Distributed Co-Simulation Lab for TSO-DSO-Customer Coordination Studies, in: 2020 AEIT International Annual Conference, AEIT, 2020, pp. 1–6.